J. Automation & Systems Engineering 3-2 (2009): 64-75

Regular paper

Ultrasound Tomography : Application to Breast and Bone Imaging

S. Mensah, P. Lasaygues

JASE
Journal of Automation & Systems Engineering

Ultrasound tomography (UT) is an imaging technique which has proved effective for soft-tissue (breast, liver, testicles…) characterization. More recently, the use of UT has been envisaged for bone imaging. In this field, the large variations of impedance distribution (high contrast) require that a finer model of wave propagation be integrated in the reconstruction scheme. Regarding echography, the main goal of UT is to provide both high contrast and resolution imaging and multi-parametric imaging (speed of sound, attenuation, stiffness tensor…). This quantitative information can be processed by Computer Assisted Diagnosis (CAD) systems. Within the frame of soft-tissue imaging, we will restrict our application to breast inspection. In the case of highly heterogeneous media such as bones, extended inversion schemes are proposed. The various reconstruction procedures are set against experiments and the image qualities are compared.

Keywords: Near-field, mammography, bone imaging.

1. INTRODUCTION

Ultrasound Tomography (UT) is an imaging technique recognized for soft-tissue (breast, liver…) characterization. More recently, the use of UT has been envisaged for bone imaging. In this domain, the large variations of the impedance distribution (high contrast) require that a finer model of wave propagation be integrated in the reconstruction scheme. In regards with Echography, the main goal of UT is to provide both high contrast and resolution imaging and multi-parametric imaging (speed of sound, attenuation, stiffness tensor…). This quantitative information can be processed by Computer Assisted Diagnosis (CAD) systems.

Within the frame of soft-tissue imaging, we will restrict our application to breast inspection. Since it improves point and contrast resolution, the use of wide band information is becoming a common practice. Besides, an efficient reconstruction procedure has to take into account the true nature of the transmitted waves (cylindrical or spherical divergence, transducer directivity) which is generally expressed in terms of near-field conditions

Recently, we have extended the tomographic procedure to data acquired in scattering configurations. For this purpose, we suppose the fluid object to be weakly heterogeneous (Born approximation) and excited by spherical waves. A new Fourier transform called the elliptical Fourier transform has been derived to solve the near-field inverse problem. It differs from the standard Fourier Transform in that a harmonic ellipsoidal wave decomposition is performed instead of a plane wave decomposition. Based on this spectral analysis, near-field tools such as near-field Radon transforms are designed. These tools make it possible to separate the impedance and the Speed of Sound (SOS) contributions and to reconstruct their cartographies.

In the case of highly heterogeneous media such as bones, extended inversion schemes are

CNRS- Laboratoire de Mécanique et d'Acoustique, Marseille, France

CNRS- Laboratoire de Mécanique et d'Acoustique, Marseille, France

proposed. A simple approach assumes a fluid-like cavity buried in an elastic cylinder surrounded by water; the refraction phenomenon on that cylinder is taken into consideration during the reconstruction. For this purpose, reflection and transmission data are processed iteratively in order to update the Green function.

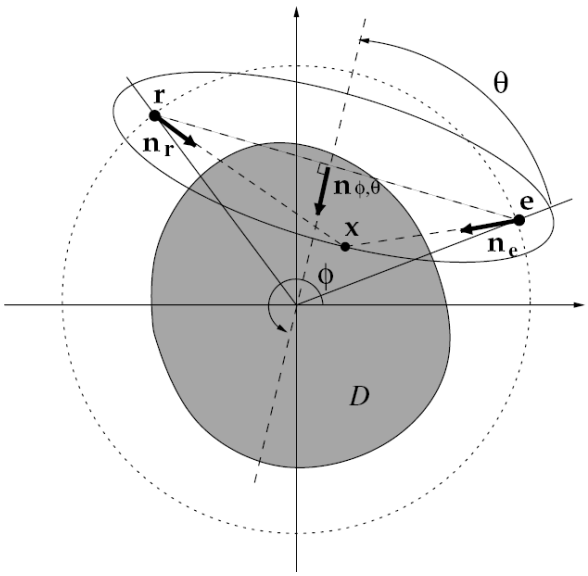

Fig. 1: Scattering acquisition configuration in acoustic tomography: the punctual source located in **e** corresponds to the focus of the spherical transmitter, the receiver focus is in **r**.

2. FORMULATION

Ultrasonic Tomography applied to soft tissues, we limit ourselves to breast inspection, has been studied in several scientific research projects [1, 2] and the use of powerful computers makes it possible nowadays to introduce enhanced algorithms [3, 4]. Numerous experimental devices have also been developed [5, 6, 7, 8]. In these approaches, breast tissues are described by means of acoustic models. Let ρ_0, c_0 be the density and SOS of the homogeneous coupling medium, let us define the contrast parameters $\alpha = (c^2 - c_0^2)/c^2$ and $\xi = Log(z/z_0)$, z is the acoustic impedance; then the governing pressure propagation equation is written:

$$-\frac{1}{c_0^2}\frac{\partial^2 p}{\partial t^2} + \nabla^2 p \equiv S \equiv -\frac{2\alpha}{c_0^2}\frac{\partial^2 p}{\partial t^2} - \nabla\alpha\nabla p + \nabla\xi\nabla p \tag{1}$$

The gland to be inspected is excited with a spherical wave having an infinite frequency band :

$$P_i(\underline{x},\underline{e},t) = \delta\left(t - \frac{|\underline{x}-\underline{e}|}{c_0}\right)\frac{1}{4\pi|\underline{x}-\underline{e}|} \tag{2}$$

Let us consider the differential distribution:

$$v_e(\underline{x},t) = -\underline{n}_e\left(\frac{1}{|\underline{x}-\underline{e}|}\delta(t) - \frac{1}{c_0}\delta'(t)\right), \tag{3}$$

unit vector $\underline{n_e}$ is shown on Fig.1, the prime stands for the first derivation. One can easily derive the integral expression of the scattered field:

$$p_d(\underline{r},\underline{e},t) = -\int_{\Sigma_t} \frac{S^*\left(\underline{x},\underline{e},t-\frac{|r-\underline{x}|}{c_0}-\frac{|\underline{x}-\underline{e}|}{c_0}\right)}{16\pi^2|r-\underline{x}||\underline{x}-\underline{e}|}\,d\underline{x} \tag{4}$$

Ellipse Σ_t of foci $(\underline{x},\underline{r})$, is defined by the relation $c_0 t = |r-\underline{x}|+|\underline{x}-\underline{e}|$. Then, $p_d(\underline{x},\underline{e},t)$ is the elliptical projection over Σ_t of the source terms. Given the two points $\underline{e}$ and $\underline{r}$, the former expression can be rewritten in its integral form marked by « $\hat{*}$ »:

$$\begin{aligned} G \,\hat{*}\, S(\underline{r},\underline{e},t) &= \int_{\Re^3} \frac{\delta\left(t-t'-\frac{|\underline{r}-\underline{x}'|}{c_0}\right)}{4\pi|r-\underline{x}'|}\; S\left(\underline{x}',\underline{e},t'\right)\; d\underline{x}'dt' \\ &= \int_{\Re^3} \frac{\delta\left(t-t'-\frac{|\underline{r}-\underline{x}'|}{c_0}\right)}{4\pi|r-\underline{x}'|}\; S^* *_{t'} p_i(\underline{x}',e,t')\; d\underline{x}'dt' \end{aligned} \tag{5}$$

Hence the synthetic expression of the scattered field (Born approximation) :

$$p_d(\underline{r},\underline{e},t) = G \,\hat{*}\, S(\underline{r},\underline{e},t) = G \,\hat{*}\, S^* *_t p_i(\underline{r},\underline{e},t) \tag{6}$$

If instead of a spherical wave of infinite bandwidth one uses a harmonic spherical transmit wave, the expression (4) becomes:

$$\begin{cases} p_d(\underline{r},\underline{e},\omega) = -\int_{\Sigma_t} \dfrac{e^{ik\left(|r-\underline{x}|+|\underline{x}-\underline{e}|\right)}}{16\pi^2|r-\underline{x}||\underline{x}-\underline{e}|} S^*(\underline{x},\underline{e},\omega)\,d\underline{x} \\ \hat{\upsilon}_e(\underline{x},\underline{e},\omega) = \underline{n}\left(\dfrac{1}{|\underline{x}-\underline{e}|}-ik\right) \\ S^*(\underline{x},\underline{e},\omega) = k^2 2\alpha - [\nabla\alpha - \nabla\xi]\;\hat{\upsilon}_e(\underline{x},\underline{e},\omega) \end{cases} \tag{7}$$

The first of these expressions reveals a transform similar in its form to the standard Fourier transform; this resemblance has caught our attention. It has the specificity of the harmonic decomposition functions having as spatial support an ellipsoid indexed with time, and for foci the locus of the transmitter and of the receiver; this decomposition has been named the *Elliptical* Fourier transform (EFT). We have shown in a previous paper [4] that this transform is invertible. Thus, the scattered field is the ellipsoidal spectrum of the secondary source term specified by the acoustical parameters.

Nota : When no confusion is possible, for any well-behaved function *f*, $f(\underline{r},\underline{e},\omega)$ refers to the spectrum of function $f(\underline{r},\underline{e},t)$. When distinction is required the spectrum is noted: $f(\underline{r},\underline{e},\omega) = \hat{f}(\underline{r},\underline{e},\omega) = \hat{f} = F\left[f(\underline{r},\underline{e},t)\right]$, *F* is the standard Fourier transform.

Then, applying the EFT (overlined with an arrow) to (5) and considering the specific derivation rules related to the elliptical analysis [4], one gets:

$$\begin{cases} \hat{\upsilon}\ (\underline{x},\omega) = \hat{\upsilon}_e\,(\underline{x},\omega) - \hat{\underline{\upsilon}}_r\,(\underline{x},\omega) \\ \underline{K} = kn_{\phi,\theta} \\ -p_d\,(\underline{K}) = k^2 2\vec{\alpha}(\underline{K}) - \left(\overleftarrow{\hat{\upsilon}_e \cdot \hat{\upsilon}}\right) * \left[\vec{\alpha} - \vec{\xi}\right](\underline{K}) \end{cases} \tag{8}$$

The scattered field is the result of the convolution in the elliptical spectral domain of the elliptical spectra with the directivity index functions. If the transmitter (resp. receiver)/pixel distances are of the order of the wavelength, we have with a good approximation

$$\hat{\upsilon}_e \cdot \hat{\upsilon}\ \approx -k^2\left(1 + \underline{n}_e.\underline{n}_r\right), \text{ where } \underline{n}_l = \nabla\left(|\underline{x} - \underline{l}|\right) \tag{9}$$

$\underline{n}_e$ is the unit vector in the direction transmitter (resp. receiver) / voxel. Then, the system is reduced to:

$$p_d\ (\underline{K}) = -k^2\left[\left(\overleftarrow{1 - n_e.n_r}\right) * \vec{\alpha} - \left(\overleftarrow{1 + n_e.n_r}\right) * \vec{\xi}\right](\underline{K}) \tag{10}$$

Indeed, these equations involve two acoustical parameters offering distinct directivity patterns that can be separated according to the spatial scanning performed:

- $\underline{n}_e = -\underline{n}_r, \quad p_d = k^2\vec{\alpha}$, in pure transmission, the scattered field is conditioned by the quadratic fluctuations of the speed of sound.
- $\underline{n}_e = \underline{n}_r, \quad p_d = k^2\vec{\xi}$, in pure reflection, the scattered field results from impedance fluctuations.

These results are coherent with those obtained using plane wave excitation and plane wave decomposition (standard Fourier transform). Here, they are extended in the sense that the analysis has been done taking into account the curvature of the "elliptical" wavefront.

A. "Near-field" tomography

By applying the inverse EFT to the elliptical spectra, it is possible to reconstruct the impedance or the sound speed maps since they are respectively obtained from pure reflection and transmission measurements.

1) Fast inversion procedure

Let $f(\underline{x})$ be a well-behaved object function defined over the compact domain *D* of $\mathbb{R}^2$. f represents one of the separable parameters specified above. For a given configuration angle $\theta = \theta_0$, (cf. figure 1), we define the elliptical Radon transform for any pair (s, ϕ) ∈ {s ∈ $\mathbb{R}$, 0≤ ϕ ≤π} by:

$$\left[R_\varepsilon f\right](s,\phi) = \int f(\underline{x})\frac{\delta\left(s - |\underline{r} - \underline{x}| - |\underline{x} - \underline{e}|\right)}{16\pi^2|\underline{r} - \underline{x}|.|\underline{x} - \underline{e}|}\,d\underline{x} \tag{11}$$

and consider the projection, $p_{\square}(s)$ under incidence ϕ :

$$\left[R_\varepsilon f\right](s,\phi)_{|\phi\ fixed} = p_\phi\,(s) \tag{12}$$

We introduce the scalar product:

$$\underline{n}_{\phi,\theta} \bullet \underline{x} = -\left(|r - \underline{x}| + |\underline{x} - \underline{e}|\right). \tag{13}$$

Here, its negative value results from the fact that the wave is propagating toward the origin, and is opposed to the outgoing orientation of the $\underline{x}$ axis.

We derive the expression of the synthesis of the function f from its ellipsoidal decomposition (the projections $p_\phi(s)$ under incidence ϕ):

$$f(\underline{x}) = \frac{1}{(2\pi)^2} \int_0^{\pi} \int_{-\infty}^{\infty} \hat{p}_\phi(S)|S| e^{i\underline{S}_\phi \bullet \underline{x}} [\underline{x}]_\phi \, dS \, d\phi . \tag{14}$$

This relation resembles the continuous expression of the classical backprojection algorithm. Excepting the normalisation term, $[\underline{x}]_\phi = 16\pi^2 |\underline{r} - \underline{x}||\underline{x} - \underline{e}|$, accounting for the divergence of the beam, one can retrieve all the constitutive elements. A difference however which is worth noticing: the nature of the projection differs since here, we consider an elliptical projection $p_\phi(s)$ over Σ_t defined by:

$$s = c_0 t = \underline{S}_\phi \bullet \underline{x} = |r - \underline{x}| + |\underline{x} - \underline{e}| \tag{15}$$

2) Elliptical Backprojection (EBP) operator

Let us consider an arbitrary function $h(s,\phi)$ where $s = \underline{n}_\phi \bullet \underline{x}$, the elliptical backprojection operator is:

$$B\left[h(s,\phi)\right](\underline{x}) = \frac{1}{2} \times \frac{1}{\pi} \int_0^{\pi} [\underline{x}]_\phi \, h\left(\underline{n}_\phi \bullet \underline{x}, \phi\right) d\phi \tag{16}$$

The function *f* is then recovered by EBP [3]:

$$f = B \circ F^{-1} \circ Abs \circ F \circ R_\varepsilon \circ f = R_\varepsilon^{-1} \circ R_\varepsilon \circ f , \tag{17}$$

where the response of filter *Abs* is $Abs(S) = |S|$.

Let us call p_{dm} the "measured scattered field" and S_{est}^* the estimated parameter map reconstructed from the data acquired. Under such conditions,

$$S_{est}^* = R_\varepsilon^{-1}\left[p_{dm}\right]. \tag{18}$$

Thus, the Elliptical Back-Propagation Algorithm leads to an Inverse Born Approximation (IBA) with a (almost) "constant background" (considering the matching of the mean acoustic impedances).

B. "Hard-tissue" tomography

In the case of hard biological tissues having larger acoustic impedances and SOS than those of the surrounding medium, the weak scattering assumption is no longer realistic. Indeed, the transmitted wave is "deviated" from its initial course because of refraction. Consequently, only a small percentage of the incident energy penetrates into the contrasted medium. Thus, due to the large sound speed and impedance fluctuations, the constant sound speed assumption in relations (4) and (5) is no more valid. Instead, one has to consider the spatial dependency of the sound speed in the derivation of the scattered field:

$$p_d(\underline{r},\underline{e},t) = -\int_{\Sigma_t} \frac{S^*\left(\underline{x},\underline{e},t+\tau(\underline{x})-\frac{|r-\underline{x}|}{c_0}-\frac{|\underline{x}-\underline{e}|}{c_0}\right)}{16\pi^2|r-\underline{x}||\underline{x}-\underline{e}|}\,d\underline{x} \quad . \quad (19)$$

Here, the temporal correction is approximated on the basis of straight line propagation inside the hard medium:

$$\tau(\underline{r},\underline{e},\underline{x}) = \frac{1}{c_0}\int_{\overline{ex}+\overline{xr}} \frac{c(\underline{x}')-c_0}{c_0}\,d\underline{x}' = \tau_e(\underline{x}) + \tau_r(\underline{x}). \quad (20)$$

Hence, the overall correction is the sum of the respective temporal corrections along the emitter-voxel (located in $\underline{x}$) path and along the voxel-receiver path.

Indeed, this correction term is unknown since the sound speed parameter is directly or indirectly sought for; it is generally estimated via an iterative tomographic procedure initialised on the basis of prior information that, for instance, may corresponds to the bone mean speed of sound for equivalent age and health status of the patient.

Then, the expression of the corrected Radon transform is:

$$\left[R_{\varepsilon c}f\right](s,\phi) = \int f(\underline{x})\frac{\delta\left(s+c_0\tau(\underline{x})-|\underline{r}-\underline{x}|-|\underline{x}-\underline{e}|\right)}{16\pi^2|\underline{r}-\underline{x}|.|\underline{x}-\underline{e}|}\,d\underline{x}. \quad (21)$$

The corrected inverse Radon transform is built from the corrected elliptical backprojection operator:

$$\left[R_{\varepsilon c}\right]^{-1} = B_c \circ F^{-1} \circ Abs \circ F \text{ , where } B_c = B\left[h\left(\underline{n}_\phi \bullet \underline{x} + c_0\tau(\underline{x}),\ \phi\right)\right]. \quad (22)$$

1) Reflection tomography

Contrast imaging, for instance the "cortical thickness" assessment in bone imaging, consists mainly in assimilating the background comprising two areas: the reference surround medium (generally water) and the homogeneous solid part (cortical bone). The default sought for corresponds to a perturbation in that cortical area.

A first practical approach in operating with reflection measurements (impedance imaging) consists in using low frequency activation in order to take advantage of the large penetration depth. In that case, the Born approximation is still satisfied since firstly the wavelength is large compared with the size of the heterogeneity and secondly, the fluctuations of the mechanical parameters inside the cavity are small. The "constant background" inversion procedure can be based on Elliptical Back-Projection algorithms (cf expression (14)) complemented by specific signal processing refinements (deconvolution). There, despite the artefacts and biases affecting the assessment of the shell thickness, good quality images may be obtained (cf figures 5, 6 and 7).

In a second approach, one can adopt the Inverse Born Approximation (IBA) with "a variable background" which consists in considering the hard medium as homogeneous while its geometry and mean SOS are unknown. It requires an iterative inversion methodology which is generally used whenever quantitative information (SOS distribution) is sought for.

2) Compound Quantitative Ultrasound Tomography

The solution that is proposed here is a mixed approach that implicitly specifies both the field inside the object and the Green function. Then starting from the expression (5), one can write the expression of the measured scattered field:

$$p_{dm}(\underline{r},\underline{e},t) = G_b \,\hat{*}\, S^* *_t\, p_b(\underline{r},\underline{e},t) \tag{23}$$

G_b is the Green function of the "variable background", and p_b is the associated field so that the total measured field is:

$$p_{tm}(\underline{r},\underline{e},t) = p_i(\underline{r},\underline{e},t) + G_b \,\hat{*}\, S^* *_t\, p_b(\underline{r},\underline{e},t)\,. \tag{24}$$

The three unknowns in the relation (23) are the Green function, the field inside the object and the contrast function S^*. These variables are assessed using the following iterative scheme:

$$\begin{cases} S_{est}^{*n} = \left[R_{\varepsilon c}^{\,n}\right]^{-1}(p_{dm}) \\ S_{est}^{*n}(\underline{x}) = \left(c^{\,n}(\underline{x}),\, \xi^{\,n}(\underline{x})\right) \\ \tau^{\,n-1}(\underline{r},\underline{e},\underline{x}) = \dfrac{1}{c_0}\displaystyle\int_{\overline{ex}+\overline{xr}} \frac{c^{\,n-1}(\underline{x}) - c_0}{c_0}\, d\underline{x}, \qquad \tau^0(\underline{x}) = 0 \\ \left[R_{\varepsilon c}^{\,n}\right]^{-1} = B_c^{\,n-1} \circ F^{-1} \circ Abs \circ F^{-1} \end{cases} \tag{25}$$

$$p_b^{n-1}(\underline{r},\underline{e},t) = p_i\left(\underline{r},\underline{e},t + \tau_e^{n-1}(\underline{r})\right) \tag{30}$$

$$G_b^{n-1}(\underline{r},\underline{e},t) = G\left(\underline{r},\underline{e},t + \tau_e^{n-1}(\underline{r})\right)$$

Nota : The last two relations are implicitly obtained but not evaluated.

To begin with, our approach aims at taking into consideration the refraction effects in order to impose (almost) straight ray propagation inside the shell. From *a priori* knowledge of the geometrical properties and of the average acoustic parameters, the incident and refracted angles are estimated using the Snell-Descartes laws. Thus, a compensation procedure has been introduced into the scanning in order to obtain parallel paths within the "homogeneous" contrasted medium.

In an iterative way, reflection and transmission measurements enable us to delineate the boundaries of the shell (the cortical region) and to assess the values of the speed of sound along the wave paths. The stop criterion corresponds to a difference between the mean velocities calculated at two different steps lower than 5 m/s.

Signal processing techniques such as deconvolution and wavelet analysis have been introduced [9] in order to enhance SOS accuracy. This iterative experimental method, described in detail in [10], known as "Compound Quantitative Ultrasonic Tomography" (CQUT), provides interesting results, but due to the operator's deep involvement, this module is not yet usable in clinical practice. Automation of the iterative process is currently under development.

3. EXPERIMENTAL IMAGING

A. Tomography system

The feasibility of UT methods was tested using our UT-scanner. When possible, UTs of bones are compared with X-ray tomographies obtained at the same cross-section.

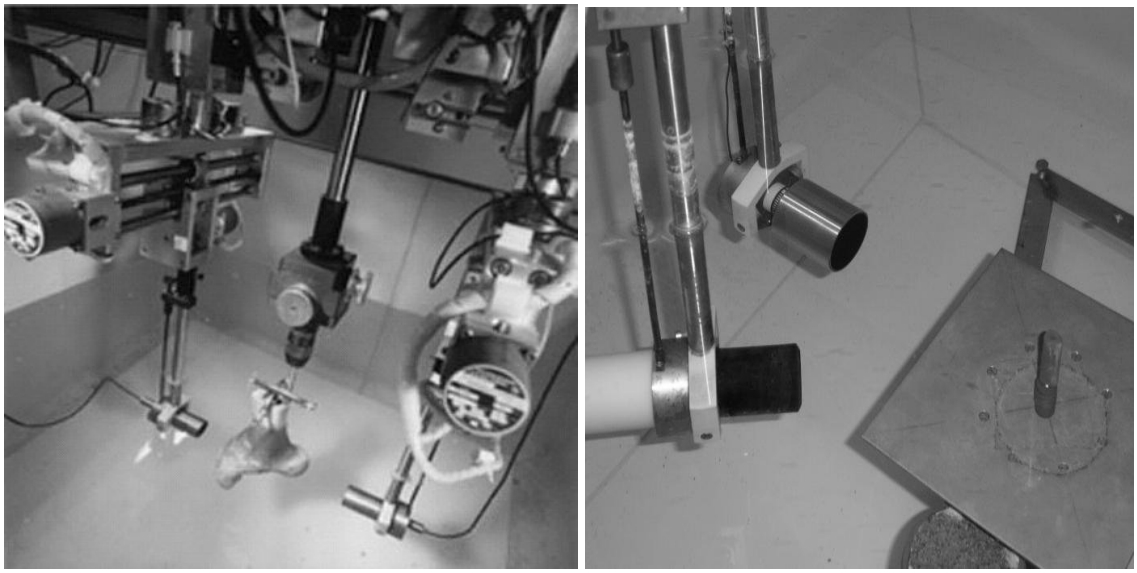

Fig. 2: The *UT*-scanner (A) transmission and (B) scattering configurations.

B. Soft-tissue experimental imaging

Figure 3 shows the reconstruction of 3 pairs of nylon wires (Ø=0.14mm) located on a circle of 30 mm, and separated by distances of 2mm, 3mm and 5mm. This illustrates the resolution of our laboratory tomographic system using 3 Mhz central frequency transducers.

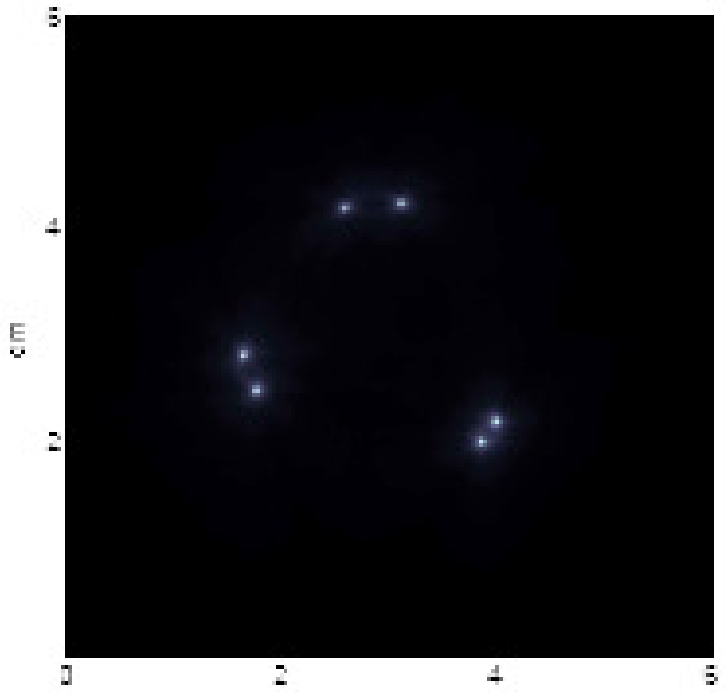

Fig. 3: Tomographic reconstruction of 3 pairs of nylon wires (Ø=0.14mm) distant of 2, 3 and 5 mm.

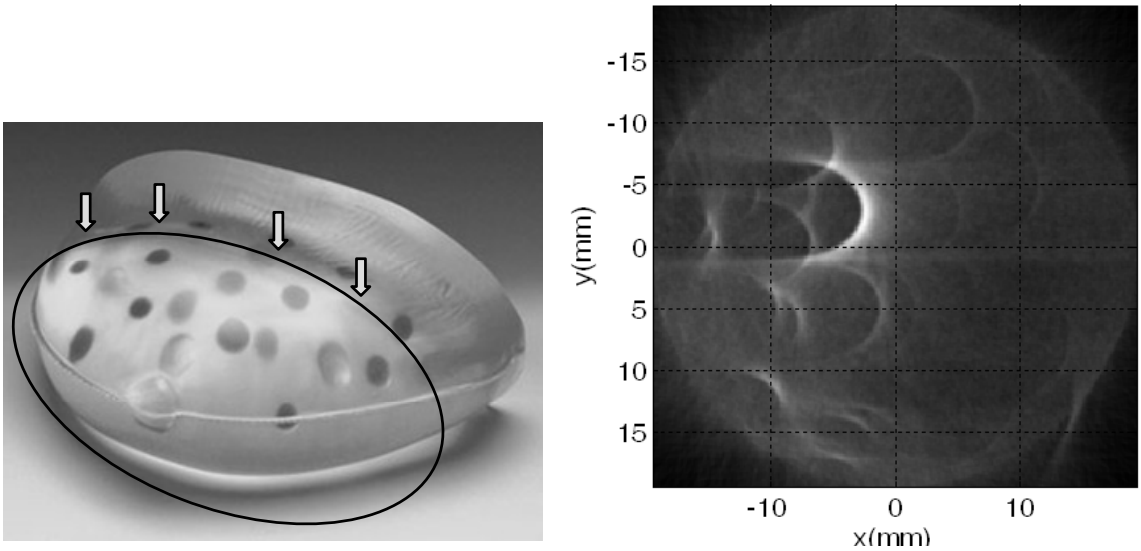

Fig. 4: Stereotactic Needle Biopsy Training Phantom Supertech ® and UT reconstruction (scanning over a 180° aperture) using 3 MHz central frequency non-focused transducer, the Region of Interest is 40 mm in diameter.

C. Bone experimental imaging.

Contrast (reflection) tomographies of bone were obtained from backscattered measurements.

Lumbar vertebra : The first example concerns the analysis of an L2 lumbar vertebra without any articular and transversal apophysis, and with a visible external spinal body diameter of approximately 30 mm (7-A). A 4-mm circular metallic rod was placed inside the specimen, perpendicular to its upper surface.

For UT (Fig. 7-B), the nominal frequency of the transducer was 500 kHz (fs=20 MHz), the reflected sinogram consisted of 180 projections (through 360°).

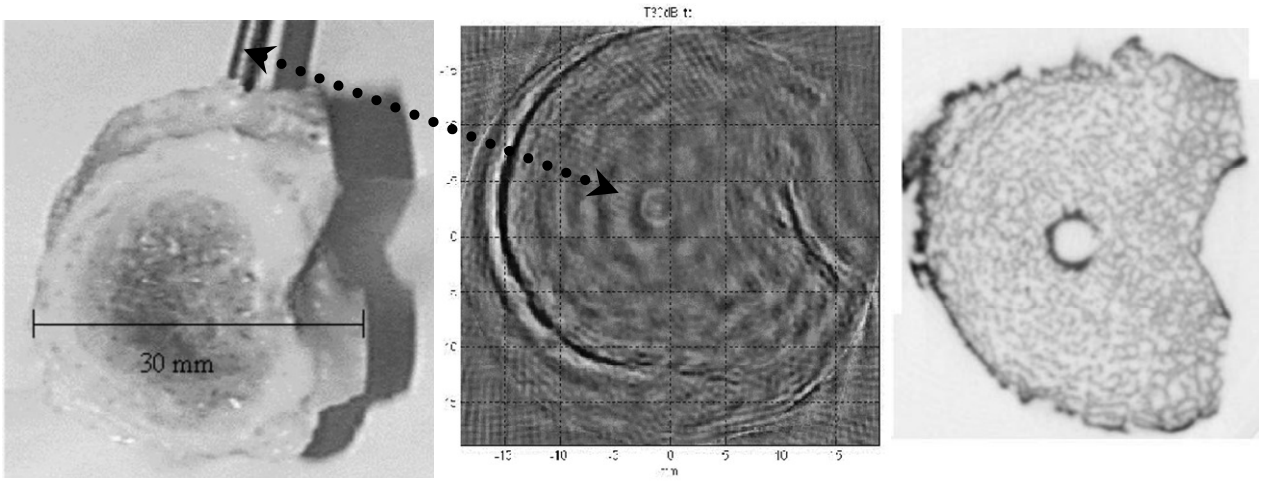

(A) (B) (C)

Fig. 5: L2 -Lumbar vertebra (A) sample picture (B) 2D-UT, Central frequency Fc = 500 kHz, 180 projections with 1024 samples, resolution 0.75 mm, image size 255 x 255 pixels (C) corresponding X-ray tomography, resolution 127 µm, image size 2304 x 3200 pixels; images (A) and (B), courtesy of [11].

The size of the image is 255 x 255 pixels. The resolution was improved using Papoulis deconvolution [11]. The resolution of the image is about 0.75 mm ($\lambda/8$).

The device used for X-ray tomography (Fig. 7-C), was composed of a Philips MG 450 radiation source, with a high intensity tube (80 keV, 10 mA). The focus size was 4.5 mm. The distance from source to object was 3 mm. A Thales Flashscan 35 was used as the scintillator imaging device (resolution 127 μm, image size 2304 x 3200 pixels).

On UT, the dimensions and the shape of the bone can be readily distinguished. The dimensions and the location of the rod are also visible and well reconstructed (see pointer). This means that on the one hand, the ultrasonic wave was propagated into the center of the scatterer despite the attenuation due to porosity and anisotropy, and, on the other hand, it was possible to discriminate a metallic implant placed in a bone structure. But it was impossible to distinguish the porous and the cortical zones, as seen from the image of the vertebra. This is an important limitation, as it makes it difficult to determine precisely from UT the ratio between the bone volume and the trabecular volume (*BV/TV*), which is the "gold standard" index of bone mineral density.

Diaphysis of an adult thighbone: In this second example, a 3D-UT of adult human female thighbones was obtained from diffraction measurements. The first sample (Fig. 8) was taken from a post-menopausal 78 year-old woman with osteoporosis, and the second (Fig. 9) from a healthy 81 year-old woman.

Fig. 8-A and Fig. 9 show the 3D-UT of the pathological and healthy thighbones. This reconstruction was obtained by superimposing sequential 2D-UT images (80 cross-sections, step 2mm). The nominal frequency of the transducers was 1 MHz. The thickness of the cross-section in the azimuth was 3 mm. The resolution and the size of the image were 0.75 x 0.75 mm and 512 x 512 pixels, respectively. The diffraction sinograms included 2048 projections, (32 incidences combined with 64 receptions).

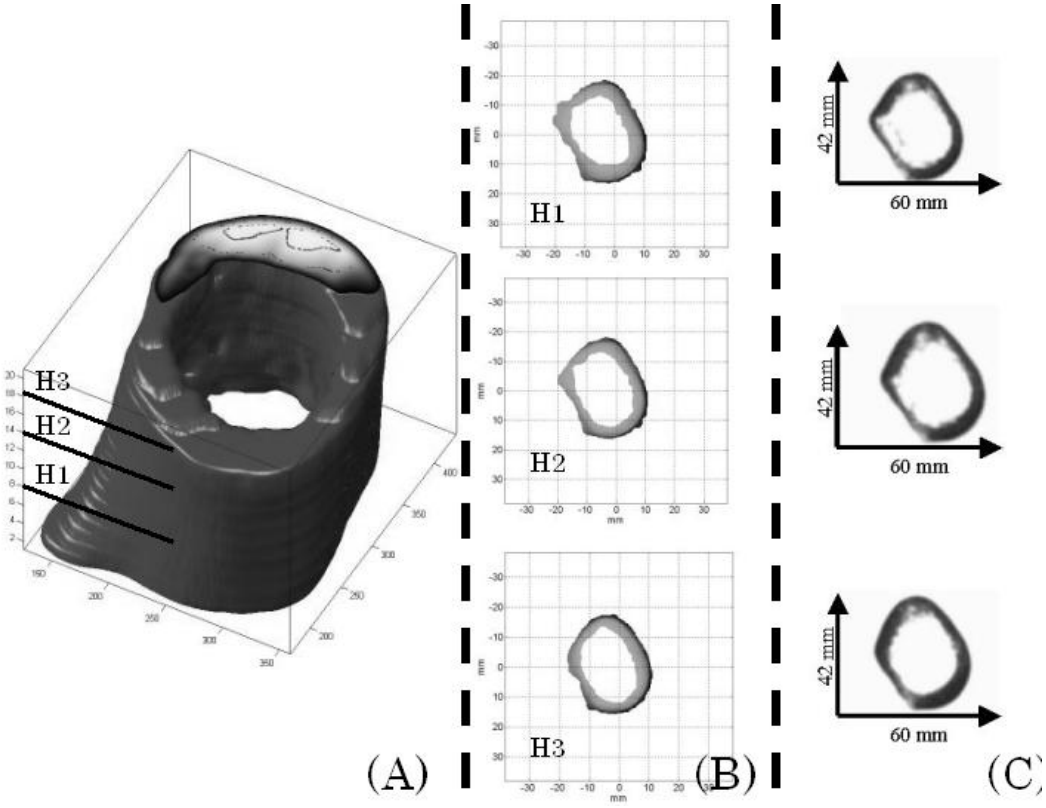

Fig. 6: Diaphysis of an adult thighbone with osteoporosis (A) qualitative image obtained with 3D-UT , (B) cross-sections, H1 = 8 mm, H2 = 14 mm and H3 = 18 mm, (C) corresponding X-ray tomographies

The General Electric® X-ray device (*CE 12000*) used provides cross-sections of 1mm thickness (resolution 0.25 x 0.25 mm, image size 512 x 512 pixels). Comparison with X-ray shows that the UT contrast image enables one to assess the cortical thickness, which is known to be a relevant risk factor regarding bone fracture. The bone thickness was indeed found to be lower for the pathological sample than for the control sample.

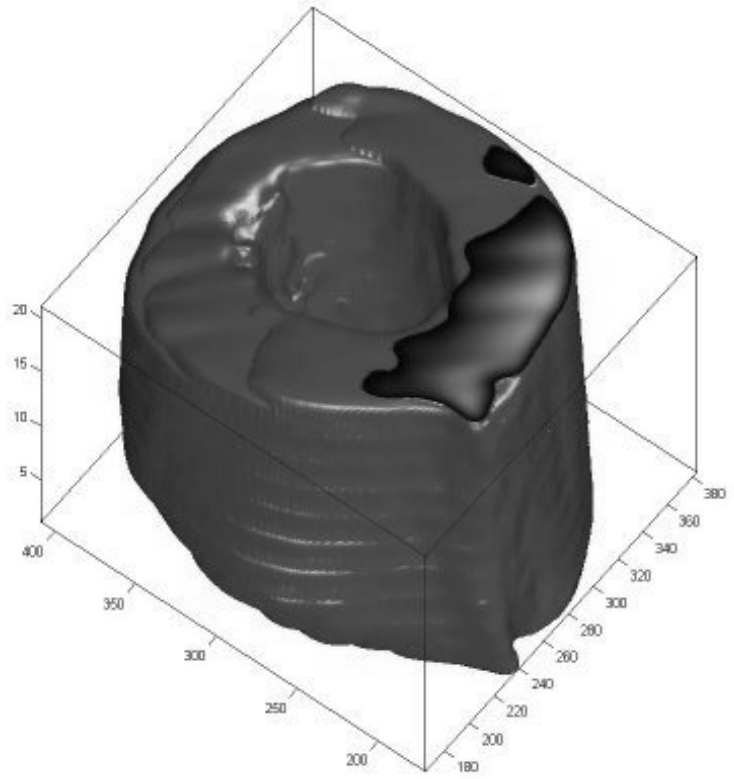

Fig. 7: 3D-UT of a healthy thighbone

4. CONCLUSION

Ultrasound Tomography (UT) appears as an alternative imaging tool able to reveal the internal structure of soft tissues (mammography) and to delineate the shape of bones (cortical thickness). The theoretical framework corresponds to the analytical formulation (Green function) of the forward problem considering point like transmitters and receivers. Thus the shape of the transmitted wave (the incident field) is spherical, as are also assumed to be the secondary sources induced by the elementary scatterers of the investigated media.

In the case of soft tissue imaging, the derivation of the near-field forward problem has led us to define new elliptical Fourier transforms and associated elliptical Radon transforms. These two transform pairs (direct and inverse transforms) enable us to separate the impedance and speed of sound contributions.

For highly heterogeneous media having larger acoustic impedances and speeds of sound than those of the surrounding medium, additional consideration of a “variable (homogeneous) background” is necessary if one seeks parametric imaging. There the strong non-linearities in the parametric distributions have been dealt with using Compound Quantitative Ultrasonic Tomography (CQUT). This procedure offers satisfactory reconstructions but still requires a noticeable involvement of the operator (time of flight extraction).

Acknowledgments

The authors are grateful for medical assistance to Drs P. Petit and J.-L. Jouve, APHM Hospitals, Marseille. This work benefited from the help of M. Talmant, M. Gindre and P. Laugier, LIP, CNRS, Paris and J.P. Lefebvre LMA, CNRS Marseille. The X tomographies were performed by F. Mazerolle LMA, CNRS, Marseille, and V. Kaftandjian LNTIR, INSA, Lyon.

References

[1] S.J. Norton and M. Linzer, "Ultrasonic reflectivity imaging in three dimensions : reconstruction with spherical transducer arrays", Ultrasonic Imaging, Vol. 1, pp. 210-231, 1979.

[2] S. Mensah and J.-P. Lefebvre, "Enhanced Compressibility Tomography", IEEE Trans. Ultrason., Ferroelec., Freq. Contr., Vol. 44, No. 66, pp. 1245-1252, 1997.

[3] S. Mensah, E. Franceschini, "Near-field ultrasound tomography", J. Acoust. Soc. Amer., vol 121, n°3, pp. 1423-1433, 2007

[4] M.P. André, H.S. Janée, P.J. Martin, G.P. Otto, B.A. Spivey and D.A. Palmer, "High-speed data acquisition in diffraction tomography system employing large-scale toroidal arrays", International Journal of Imaging System and Technology, Vol. 8, No. 1, 137-147, 1997.

[5] S.A. Johnson, D.T. Borup, J.W. Wiskin, F. Natter, F. Wuebbling, Y. Zhang and C. Olsen, "Apparatus and Method for Imaging with Wavefields using Inverse Scattering Technique", *US Patent* 6, 005, 916, 1999.

[6] P. Lasaygues, D. Tanne, S. Mensah and J.-P. Lefebvre, "Circular antenna for breast ultrasonic diffraction tomography", Ultrasonic imaging, Vol. 24, pp. 135-146, 2002.

[7] R.C. Waag and R.J. Fedewa, "A ring transducer system for medical ultrasound research", IEEE Trans. Ultrason., Ferroelec., Freq. Contr., Vol. 53, No. 10, pp. 1707-18, 2006.

[8] P. Lasaygues, J.P. Lefebvre and S. Mensah, "Deconvolution and wavelet analysis on ultrasonic reflexion tomography", Topics On Non Destruct Eval. Series B. Djordjevic and H. Dos Reis, Series Editors, 3, III Inter Work. – Adv. in Signal Process for NDE of Mater, in X. Maldague, Vol. 3 Tech Ed, pp. 27-32, ASNT, 1998.

[9] E. Ouedraogo, P. Lasaygues, J.-P. Lefebvre, M. Gindre, M. Talmant and P. Laugier, "Contrast and velocity ultrasonic tomography of long bones", Ultrasonic Imaging, Vol. 24, pp. 135-146, 2002.

[10] P. Lasaygues and JP. Lefebvre, "Cancellous and cortical bone imaging by reflected tomography," Ultrasonic Imaging, Vol. 23, pp. 55-68, 2001.